Astron. Astrophys. 324, 641–650 (1997)

ASTRONOMY
AND
ASTROPHYSICS

Multi-frequency radio spectral studies of the supernova remnant G78.2+2.1

X. Zhang[1], **Y. Zheng**[1], **T.L. Landecker**[2], **and L.A. Higgs**[2]

[1] Beijing Astronomical Observatory, Chinese Academy of Sciences, Beijing 100080, China
[2] Dominion Radio Astrophysical Observatory, National Research Council, P.O. Box 248, Penticton, British Columbia V2A 6K3, Canada

Received 10 January 1997 / Accepted 14 February 1997

Abstract. A new map of the SNR G78.2+2.1 at 232 MHz is presented. This map is used with other images at 408, 1420, 2695 and 4800 MHz to investigate the total spectral index of the SNR and the variation of spectral index across it. The integrated spectral index is $\alpha = 0.54 \pm 0.02$ (where $S_\nu \propto \nu^{-\alpha}$). Maps of the spectral-index variation across the source are derived using a method which calculates a differential spectral index. This method is independent of offset errors and large-scale background variations. Systematic spectral-index variations of $\sim \pm 0.15$ are found, consistently in the many independent pairs of data sets. Regions of higher spectral index (steeper spectra) appear around the periphery of the remnant and in its central area. Regions of lower spectral index (flatter spectra) are also found within the remnant. The latter may result from a change in the nature of the non-thermal emission or may represent "contamination" from underlying patches of thermal emission. There is no clear correlation of spectral index with intensity across the SNR. Theoretical reasons for spectral-index variations have been explored but no clear interpretation of the apparent spectral steepening near the shock front has been found nor has an explanation of the steep-spectrum central region.

Key words: ISM: supernova remnants – ISM: individual objects: G78.2+2.1

1. Introduction

The galactic object G78.2+2.1 was first identified as a supernova remnant (SNR) of the shell type by Higgs et al. (1977) from observations made with the DRAO Synthesis Telescope at 1420 MHz (Roger et al. 1973). Continuum images of the SNR have been made since at a number of radio frequencies. Zheng (1989) observed the remnant with the Miyun Synthesis Radio Telescope (MSRT) at 232 MHz, finding a total flux density of 580 Jy at 232 MHz, and a spectral index of ~ 0.4 between 232 and 1420 MHz. Pineault & Chastenay (1990) and Wendker et al. (1991) presented maps of G78.2+2.1, obtained with the DRAO Synthesis Telescope at 408 MHz (Veidt et al. 1985). At higher frequencies, maps of the region have been made by Fürst et al. (1990) at 2695 MHz, by Wendker (1984) at 4800 MHz, and by Higgs (1977) at 10 GHz. Wendker et al. (1991) derived a spectral index of $\alpha = 0.52$ (where $S_\nu \propto \nu^{-\alpha}$) from the integrated flux densities at 408, 1420 and 4800 MHz.

The remnant is located in a complex area of the galactic plane where the line of sight is along the local spiral arm. Landecker et al. (1980) observed H I in the region around the SNR. The distance to G78.2+2.1 was estimated as 1.5 kpc on the basis of H I absorption of the brightest continuum structures. Associations between the remnant morphology and various H I structures were demonstrated, and high-velocity H I , probably accelerated by the SNR, was discovered. Further observations of H I in the direction of G78.2+2.1 (Braun & Strom 1986) showed that many low-level H I features displayed a strong morphological resemblance to the radio continuum structure. Interaction of the SNR with molecular gas was revealed in the CO observations of Fukui & Tatematsu (1988). Higgs et al. (1983) reported that analysis of Einstein Observatory X-ray data showed weak X-ray emission which morphologically resembled the radio continuum structure.

In this paper we present a new map of G78.2+2.1 at 232 MHz, and combine it with existing data at 408, 1420, 2695 and 4800 MHz. We demonstrate that there are small, but significant, variations of spectral index across the remnant.

2. Observations and data reduction at 232 MHz

The SNR G78.2+2.1 was first observed at 232 MHz using the Miyun Synthesis Radio Telescope (MSRT) by Zheng (1989). Since those observations were made, technical improvements have been made on the telescope and in the data reduction methods. The remnant was observed again in the course of the Miyun All-Sky Survey (Zhang et al. 1993). The result is a new map of G78.2+2.1 with improved dynamic range; this is the best low-frequency map with high angular resolution available.

Send offprint requests to: L.A. Higgs

Table 1. Details of observations with the Miyun Synthesis Telescope

Dates of Observation:		1993 June 8
Field Centre (1950):	R.A.	$20^h\ 15^m$
	Dec.	$43^\circ\ 00'$
Observing Frequency:		232 MHz
Number of Antennas:		28
Antenna Diameter:		9 m
Field of View:		$10^\circ \times 12^\circ$ at 50%
Synthesized Beam:		$4.0'$ (EW) $\times$ $6.0'$ (NS)
Baseline Coverage:		18 to 1164 m
Baseline Increment:		6 m
Number of Baselines:		192
Receiver Noise:		100 K
Bandwidth:		1.5 MHz
Correlator:		96-baseline, 1-bit digital, with digital path compensation
Sample Time:		10 s
Visibility Noise:		10 Jy/baseline/sample
Polarization:		linear
Calibrator:		Cyg A (7944 Jy)

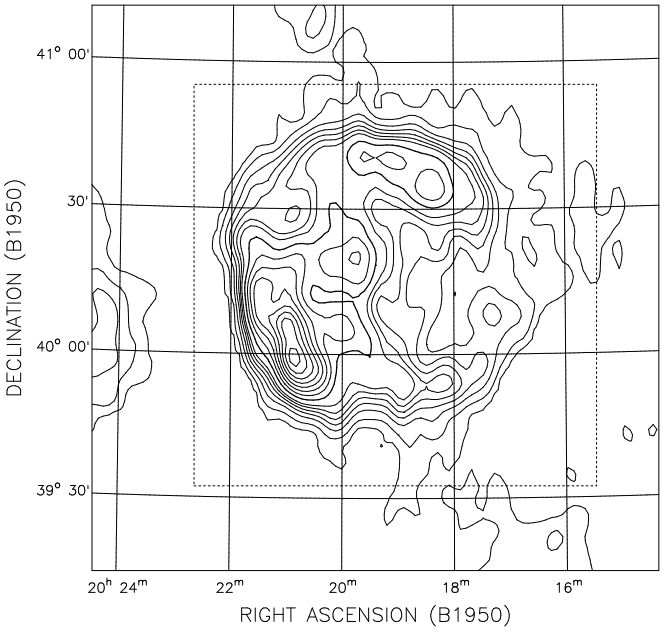

Fig. 1. Brightness-temperature map of G78.2+2.1 at 232 MHz. The contour levels are (in Kelvins): 100, 250, 500, 750, 1000, 1250, 1500, 2000, 2500, 3000, 3500, 4000, 4500, 5000 and 5500. Every second level is plotted with a heavier line, and the 2000-K contour is accentuated more. The resolution is $4.4'$ (R.A.) $\times$ $6.0'$ (Dec.), and a brightness temperature of 1000 K is equivalent to 4.2 Jy/beam. The dotted square outlines the area used elsewhere in this paper for T–T plots (except Fig. 2).

Table 1 shows the telescope parameters for this observation. A general description of the data reduction process for Miyun data can be found in Zhang et al. (1993). The MSRT includes east-west baselines from 18 m (14λ) to 1164 m (902λ). Since shorter baseline data are missing, the observation of an object as large as G78.2+2.1 requires correction for the missing data. As no large single antenna is available at 232 MHz, a fitting method based only on the synthesis telescope data has been developed (Zhang 1995). This kind of fitting was pioneered by Braun & Walterbos (1985); the method is based on a direct calculation of the visibilities for the missing short spacings from CLEAN components derived from the synthesis telescope data. The flux density and broad structure are successfully recovered by this procedure. The resulting 232-MHz brightness-temperature map of G78.2+2.1 is shown in Fig. 1, after convolution to a resolution of $4.4'$ (EW) $\times$ $6.0'$ (NS) (to facilitate comparison with other observations). The appearance of the SNR agrees very well with that seen at other frequencies. Some low-level thermal emission from the H II region IC 1318b can be seen at the eastern edge of the map, and from other H II regions north and south of the SNR.

3. Measurement of spectral-index distribution

The integrated spectrum of G78.2+2.1 has been studied by Higgs et al. (1977), by Zheng (1989) and by Wendker et al. (1991). Both Zheng (1989) and Wendker et al. (1991) mentioned that the spectral-index variation across the source is less than$\pm$ 0.1. These studies were based on the comparison of integrated flux density at different frequencies. This method is limited, at least in this case, by the difficulty of determining the background level in the complicated surroundings of the SNR. The accuracy of this method is further limited by the difficulty of establishing the zero level of observations at a number of frequencies. An error in the zero level manifests itself as a spectral-index variation which appears to correlate with intensity.

In this paper we determine *differential* spectral indices using a variation of the *T–T plot* method, which has been used, for example, to demonstrate that variations of spectral index exist in the Cygnus Loop (Green 1990) and HB9 (Leahy & Roger 1991). In this approach, first applied by Costain (1960) and Turtle et al. (1962) to data of very low angular resolution, within a selected area on the sky (analysis box) the brightness temperature (Y), T_1, at one (lower) frequency is plotted against the brightness temperature (X), T_2, at a second (higher) frequency. Linear regression is used to calculate the best fit to the data, and the slope of the fitted line gives the differential spectral index. The size of the box is arbitrary, but it should be considerably larger than the effective angular resolution of the data, since the method requires temperature variation within the box. The advantage of this method is that the result is minimally affected by zero-level errors in the data. Furthermore, the zero level of the data can wander slowly across the image without introducing significant errors.

As an illustration of the basic T–T plot method and its strengths and weaknesses, Fig. 2 shows a T–T plot made us-

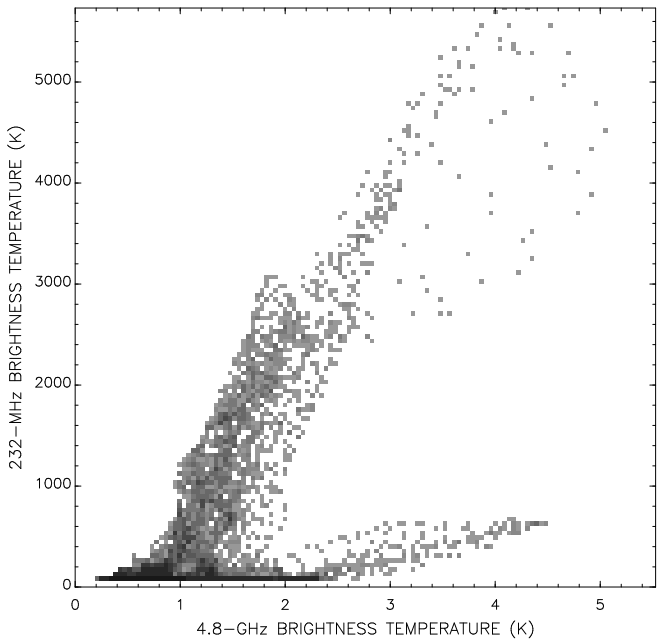

Fig. 2. The T–T plot obtained by comparing the 232-MHz data in Fig. 1 with the 4800-MHz map of the same area. The gray scale indicates the density of points in the plot. The details of this distribution are discussed in the text.

ing all the data in Fig. 1 and an equivalent map at 4800 MHz, obtained by convolving the data of Wendker (1984) to match the 232-MHz resolution. The prominent diagonal distribution of points in Fig. 2 represents the non-thermal emission from the SNR, while the prominent branch lying just above the X axis represents thermal emission from the surroundings of the SNR. Where non-thermal and thermal emission processes overlap spatially, T–T plots become more confused. There is a bright thermal source, the γ-Cygni Nebula, which is embedded in the bright south-eastern filaments of the SNR (and may or may not be physically related to the SNR). The presence of this thermal source is indicated by the scatter of points to the right of the top half of the non-thermal branch in Fig. 2. (Where thermal and non-thermal temperature variations both exist, the points in the T–T plot are the result of adding a non-thermal "vector" and a thermal "vector"). From this, one can see that the γ-Cygni Nebula sits on a 232-MHz non-thermal backround that varies from $\sim$ 2500 K to 5000 K. Conversely, the width of the non-thermal branch, especially below 3000 K, indicates that the SNR is superimposed on a 4.8-GHz thermal background that varies by $\sim$ 1 K. Recognition of these subtleties in interpretation of T–T plots is important.

We have developed, following Anderson & Rudnick (1993), an extension of the T–T plot method which we call the *convolution differential-spectral-index* technique. The analysis box within which the linear regression is calculated is moved across the image in steps of one pixel, and at each position of the analysis box, three values are computed: the slope of the fitted line, the error in the slope, and the Y-axis intercept of the line. This produces three output arrays: an image of differential spectral index, an image of the error in the regression, and an image related to the zero offsets in the temperature scale. Biasses which are constant across the map are eliminated, and the effect of baselevel variations on scales smaller than the box size appears in the regression error. One must emphasize the fact, however, that a method such as this yields the spectral index of the emission that is varying most within the analysis box. Thus a weak but spatially varying thermal source, superimposed on a much stronger but non-varying non-thermal source will produce a spectral index which is thermal even though the bulk of the emission at that point is non-thermal.

The assessment of regression errors is important. If the points in a T–T plot are distributed in a long, narrow strip, the regression will give an accurate result. However, in a region where variations in brightness temperature are small and are dominated by noise or in a region where both thermal and non-thermal variations are appreciable, the distribution of points will tend to fill a trapezoid and the fitting of a linear regression is imprecise. In order to estimate the slope and error in the slope of a line fitting data in which both X and Y values have errors (either due to noise or a mixture of inherent spectral indices), the regression is done twice, once assuming Y to be a function of X, and once assuming X to be a function of Y. The average slope is then used and the error in the average slope is taken to be one half the difference in the two slopes or the statistical error in the average (based on the formal statistical errors of both fits), whichever is larger. If the statistical error in one of the fits exceeds 0.06 (in spectral index), the former has usually been used.

Five maps of G78.2+2.1 are used in this paper to study the variation of spectral index across the SNR. Details of these are given in Table 2. All have first been converted to brightness-temperature units and then convolved to the standard resolution of $4.4' \times 6.0'$.

4. Results

4.1. Integrated spectral index

From the map of Fig. 1 we obtain an integrated flux density of 670 ± 50 Jy at 232 MHz for G78.2+2.1 (this value is tied to the flux density scale of Baars et al. (1977) by the value adopted for the flux density of the calibrator, Cyg A – see Table 1). By comparing this with the 4800-MHz value, 150 ± 15 Jy (Wendker et al. 1991), we obtain a spectral index of 0.49 ± 0.05. However, both of these flux densities include thermal and non-thermal emission from within the boundary of the SNR, and the derived spectral index does not necessarily represent the SNR emission alone.

By separating the 232-MHz map and 2695-MHz map into thermal and non-thermal components, following the method described by Higgs et al. (1977), the flux density of the γ-Cygni Nebula was estimated to be 8.5 Jy at 232 MHz and 5.5 Jy at 2695 MHz, implying a spectral index of $\sim$ 0.15. In all further

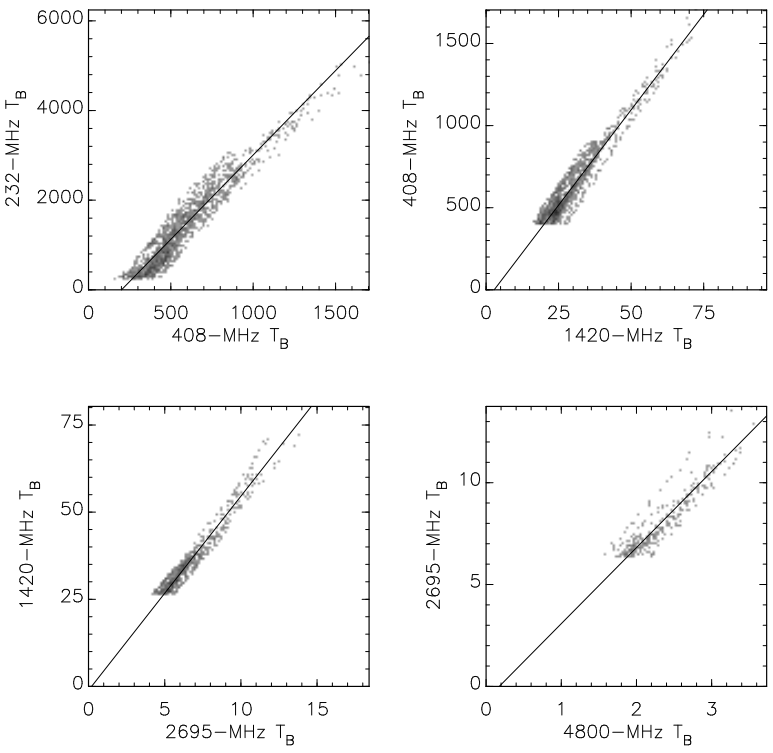

Fig. 3. Sample T–T plots of the whole SNR (above selected lower-frequency cut-off temperatures) for various frequency combinations. The best-fitting straight lines, corresponding to the spectral indices in Table 3, are shown.

Table 2. Observations used in the study of spectral index

Frequency (MHz)	Telescope	Angular Resolution (arcmin)	Reference
232	Miyun Synthesis Telescope	4.0 × 6.0	This paper
408	DRAO Synthesis Telescope	3.5 × 5.2	Wendker et al. (1991)
1420	DRAO Synthesis Telescope	1.0 × 1.5	Gray & Landecker (1997)
2695	Effelsberg 100-m	4.4	Fürst et al. (1990)
4800	Effelsberg 100-m	2.6	Wendker (1984)

analysis, the region of the γ-Cygni Nebula has been excluded from the calculations.

Table 3 gives the integrated spectral indices obtained by the T–T plot method from the ten possible frequency combinations. For each plot, a lower-frequency brightness temperature cut-off was selected such that all areas of thermal emission from outside the periphery of the SNR were eliminated from the analysis. This does not, of course, necessarily eliminate thermal contributions within the area of the remnant. These cut-off temperatures are listed in the table. The linear fits, for this table, were made by equally weighting occupied pixels in a T–T plot image, i.e. a "uniform" weighting that emphasizes the shape of the T–T distribution rather than "natural" weighting that gives every T_1/T_2 pair equal weight. Fig. 3 shows some of the T–T plots from which the spectral indices in Table 3 were derived. The weighted mean of the values in Table 3 is 0.54 ± 0.02. Because of the varying lower-frequency T_B cut-offs, different plots "sample" different intensity levels of the non-thermal emission. There is a suggestion in the data of Table 3 (by comparing successive rows of the table) that the spectrum of the higher-intensity SNR emission is slightly steeper than that of the lower-level emission. Similarly, by comparing columns, there is a suggestion that the spectral index decreases somewhat at lower frequencies. Such an effect might be due to absorption in ionized gas along the line of sight to the SNR. On the other hand, plots such as these are critically dependent upon the accuracy of the brightness-temperature scales of the various observations. It can be shown that the entries in Table 3 can all be made consistent with a nominal spectral index of 0.50 if each of the input observations are "corrected" for a scale error. The required corrections are: 232 MHz × 1.037; 408 MHz × 0.959; 1420 MHz × 0.986; 2695 MHz × 1.102; and none at 4800 MHz. These are generally small (except at 2695 MHz) and could represent valid scale corrections at all frequencies other than 2695 MHz. Indeed, there is some evidence (Landecker et al. 1996) that the 408-MHz data (Wendker et al. 1991) are (10 ± 6)% too bright. In any case, for the following analysis of spectral-index variations over the

Table 3. Derived spectral indices from T–T plots of whole SNR

High Freq.:		408 MHz	1420 MHz	2695 MHz	4800 MHz
Low Freq.	Cut-off				
232 MHz	260 K	0.35 ± 0.08	0.48 ± 0.06	0.52 ± 0.04	0.49 ± 0.05
408 MHz	400 K		0.52 ± 0.03	0.57 ± 0.02	0.52 ± 0.04
1420 MHz	26.5 K			0.68 ± 0.05	0.50 ± 0.06
2695 MHz	6.4 K				0.32 ± 0.16

SNR, the above corrections will be applied in order to ensure uniformity in the presentation of results.

4.2. The variation of spectral index across the SNR

Using the convolution differential-spectral-index method described above, we have calculated maps of the spectral index across the SNR. Maps for all combinations of frequencies were produced. An analysis box of $18' \times 23.3'$ ($\sim 4 \times$ resolution) was used. (A smaller analysis box was also used, increasing somewhat the "resolution" of the spectral variations, but gave essentially the same large-scale results as discussed below). Within the analysis box, individual T_1/T_2 pairs were weighted according to a Gaussian function, of half-width of $13.5'$, in order to give the convolution process a Gaussian-like smoothing effect. It must be noted that one cannot strictly define the effective resolution that results from the convolution differential-spectral-index method. For example, if there is only one feature that is varying in intensity, with a given α, within the analysis box, the effective resolution is given by the size of the analysis box. However, if there are two spatially varying features, with different α values, within the analysis box, the effective resolution is dictated more by the Gaussian weighting. The result is that distributions of spectral index derived in this manner will have an indeterminate effective resolution, However, in the following, an effective resolution of about $14.5'$ will be assumed.

The results are presented in Figs. 4 – 8, where each figure presents two maps, each using independent observations. In Fig. 4, the frequency ratio used for the two maps is about 11.7; for Figs. 5 and 6 it is about 5 (3.4–6.6); and for Figs. 7 and 8 it ranges from 1.8 to 3.5. In each map, the differential spectral index is shown only where the error in its determination is less than 0.06. Although all of the maps in these figures differ in detail, certain major features appear to be consistently present. In order to enhance these, an average spectral-index distribution was computed using all pairs of frequencies, weighting the spectral index at each point of the maps in Figs. 4 – 8 inversely proportional to the square of the error of its determination. This distribution is presented in Fig. 9, along with 232-MHz brightness-temperature contours after equivalent smoothing.

First, there is a region of higher spectral index near the projected centre of the SNR. The average peak position of this is R.A. = $20^{\rm h}\ 19^{\rm m}$, Dec. = $40^\circ\ 15'$ (1950), and the region is probably several arc-minutes in size and seems to be part of a "bar" of steeper emission across the remnant. Its apparent spectral index (after the overall normalization to 0.5) is 0.70 ± 0.05. It lies slightly to the west of a small patch of enhanced SNR emission, peaking at R.A. = $20^{\rm h}\ 19^{\rm m}\ 40^{\rm s}$, Dec. = $40^\circ\ 20'$ (1950) in Fig. 1.

Secondly, there are regions of steeper spectra around the outer periphery of the remnant, generally on the outward side of the peak radio emission. Two regions appear prominently in most of the maps: one near R.A. = $20^{\rm h}\ 20^{\rm m}$, Dec. = $40^\circ\ 44'$, and one just to the east of the γ-Cygni Nebula, near R.A. = $20^{\rm h}\ 21^{\rm m}\ 30^{\rm s}$, Dec. = $40^\circ\ 00'$. These, and other steep-spectrum patches that appear in some of the maps, all lie near the expected shock boundary with the surrounding interstellar medium. The spectral indices in these areas appear to be > 0.6.

Finally, there are regions of lower than average spectral index (< 0.5) at regions lying between the central steep-spectrum region and those at the outer periphery. These appear to lie on the inward side of the regions of most intense SNR emission. Two of the more prominent areas with flatter spectra are: near R.A. = $20^{\rm h}\ 20^{\rm m}\ 40^{\rm s}$, Dec. = $40^\circ\ 14'$, with $\alpha = 0.46 \pm 0.02$; and near R.A. = $20^{\rm h}\ 18^{\rm m}\ 55^{\rm s}$, Dec. = $40^\circ\ 30'$, with $\alpha = 0.39 \pm 0.03$.

There are a few extragalactic radio sources lying within the periphery of the supernova remnant, but the steeper-spectrum areas are probably not the result of such "contamination". The strongest of these sources are (*a*) one near R.A. = $20^{\rm h}\ 17^{\rm m}\ 15^{\rm s}$, Dec. = $40^\circ\ 09.0'$, and (*b*) one near R.A. = $20^{\rm h}\ 19^{\rm m}\ 34^{\rm s}$, Dec. = $40^\circ\ 39.5'$. These are both about 0.4 Jy at 1420 MHz (Gray & Landecker 1997). With a typical extragalactic spectral index, they could each contribute about 1.4 Jy at 232 MHz (or about 330 K in brightness temperature). There may be a hint of the effect of the former of these in some of the maps in Figs. 6, 7 and 8.

From the consistency of the large-scale spectral variations in Figs. 4 to 8, based on five independent radio observations, the reality of these variations ($\sim \pm 0.15$) cannot be doubted. Whether they represent real variation in the spectrum of non-thermal emission is another question. Clearly it is possible that variations in underlying thermal emission can result in regions of lower, well determined, differential spectral index, if the thermal emission within the analysis box varies more rapidly than the non-thermal emission. We have constructed synthetic maps of a model source approximating G78.2+2.1, at frequencies of 232 MHz and 2695 MHz. The model consisted of a Gaussian non-thermal ring of spectral index 0.5, with a peak brightness temperature of 29 K at 1420 MHz. Underlying this were three

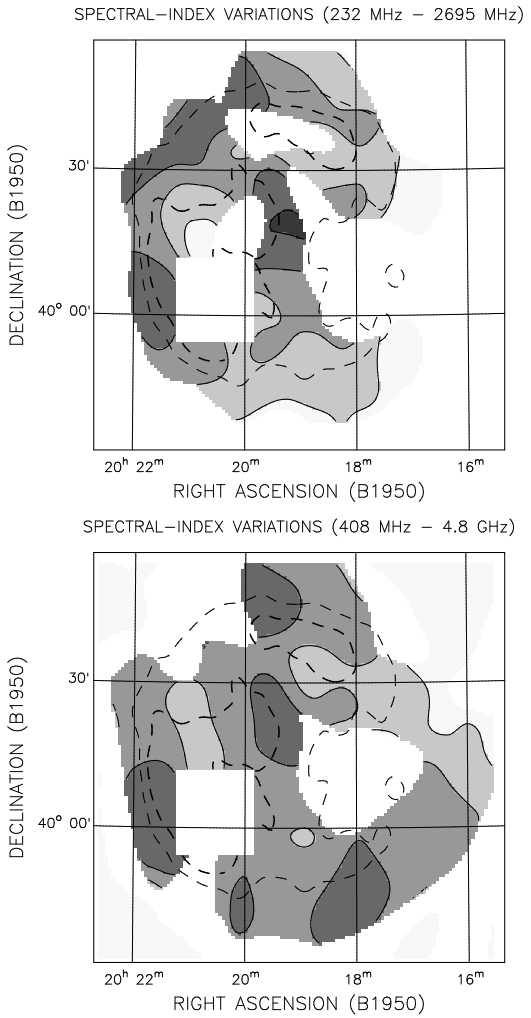

Fig. 4. Maps of differential spectral index. Areas in white arc regions in which the error of the derived spectral index exceeds 0.06, or the region around the γ-Cygni Nebula which has been blanked out. The six shading levels denote the following ranges of spectral index: (darkest) > 0.8; 0.8 to 0.7; 0.7 to 0.6; 0.6 to 0.5; 0.5 to 0.4; (lightest) < 0.4. For reference, the dashed lines indicate the 750-K and 2000-K contours from Fig. 1. (The spectral-index distribution is somewhat more extended than the contours of Fig. 1 because of the [uncertain] smoothing that results from the convolution process). In this figure, the frequency ratio is about 12:1.

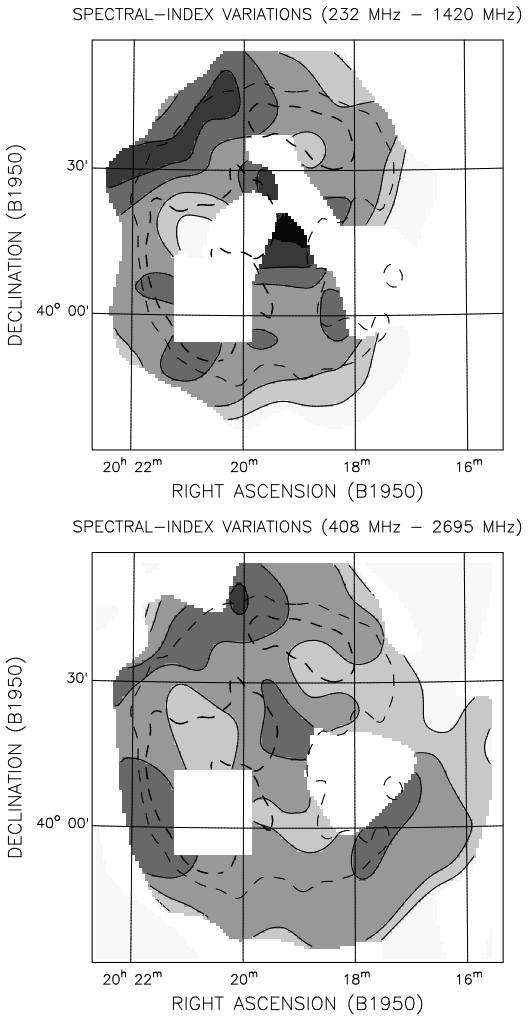

Fig. 5. Maps of differential spectral index where the frequency ratio is in the range of (6.1 – 6.6):1. Details are the same as for Fig. 4.

Gaussian (half-widths ranging from $9'$ to $12'$) thermal patches of emission (spectral index of 0.1) with peak brightness temperatures ranging from 5 K to 7.5 K at 1420 MHz. When processed in the same fashion as the real data, patches of differential spectral index in the range 0.25 to 0.40 were obtained, with small uncertainties. Thermal features of this size cannot easily be ruled out – they correspond to background features of less than 0.6 K at 4800 MHz and it was noted that Fig. 2 indicated thermal variations of more than this magnitude underlying the SNR. In fact, the 1420-MHz "thermal" component underlying the remnant derived by Higgs et al. (1977) has a 17-K peak very close to one of the flatter-spectrum areas noted above. On the other hand, the location of these regions of lower spectral index just inward from the most intense non-thermal emission is suggestive of a change in the spectrum of the non-thermal emission.

4.3. The variation of spectral index with intensity

Using the data in Fig. 9, any relationship between spectral index and intensity was investigated. The 232-MHz brightness temperature was plotted against average spectral index, using all positions in the image where the average spectral index included at least one well-determined value. This distribution is shown in Fig. 10, where brightness-temperature spectral index $(2 + \alpha)$ is the abscissa. No clear trends of spectral index with intensity are seen. The loop-like structures at temperatures between 1000 and 2000 K probably originate from the differing smoothing procedures used for the temperatures (Gaussian convolution) and spectral indices (weighting the points in the correlation analysis with a spatial Gaussian). Below an intensity of 800 K, there appears to be a mixture of thermal and non-thermal

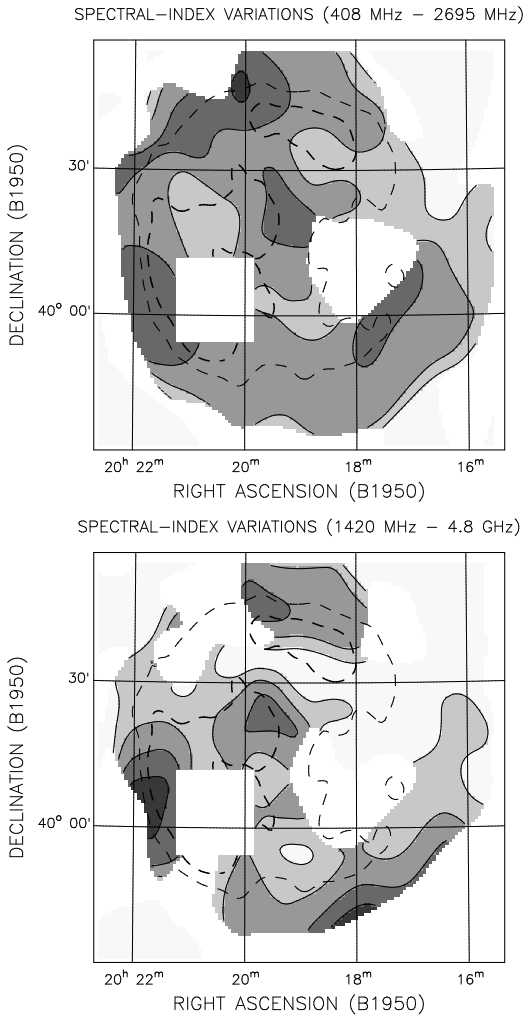

Fig. 6. Maps of differential spectral index where the frequency ratio is in the range of (3.4 – 6.6):1. Details are the same as for Fig. 4.

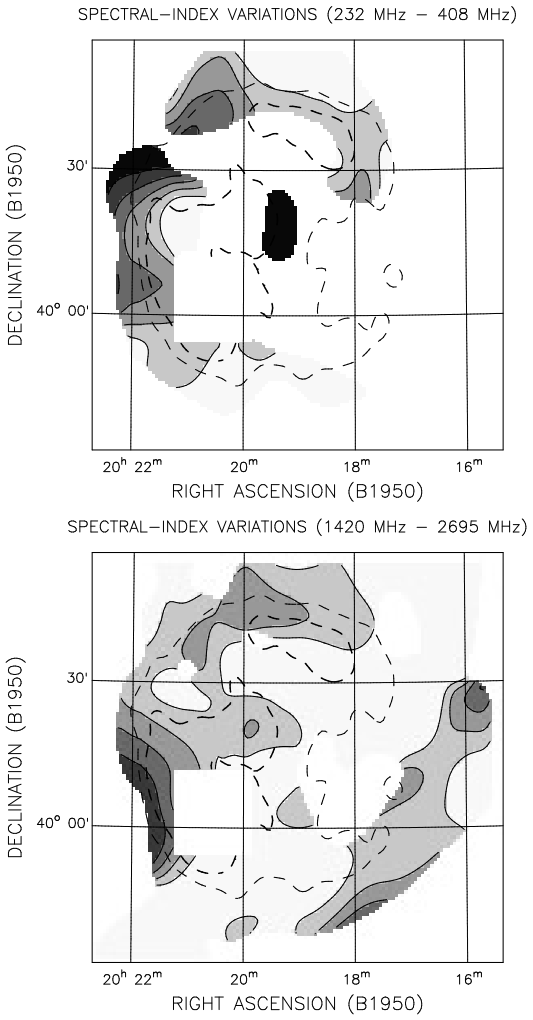

Fig. 7. Maps of differential spectral index where the frequency ratio is about 1.8:1. Details are the same as for Fig. 4.

emission, varying on similar size scales, which may be related to the areas of lower spectral index noted above. Above 800 K, there appear to be two main "components": a dominant component with α varying from ~ 0.55 to ~ 0.45 with increasing intensity, and a less prominent component at $\alpha \sim 0.61$.

5. Possible interpretations of the spectral-index variation

The spectral-index features shown in Fig. 9 show some symmetry about an axis through the centre of the remnant, at a position angle of $\sim 40^\circ$, influenced rather strongly by the bar of steeper spectral index across the SNR. The SNR emission itself shows fairly strong bilateral symmetry around the same axis (see Fig. 1). This leads to the conclusion that the observed spectral-index variation is inherent to the SNR and is not produced by superimposed thermal-emission variations from unrelated regions along the line-of-sight, either in front of or behind the SNR. On the other hand, the central steep-spectrum region lies on the edge of a bright non-thermal (Higgs et al. 1977) emission patch, which probably lies in the shell of the SNR, not physically in the centre of the object. If the steeper-spectrum emission is related to this patch, it may be arising in the shell and the above symmetry argument may have less weight.

Spectral-index variations have been reliably detected in a number of shell SNRs. Anderson & Rudnick (1993) have made a succinct summary of the findings to date, and they separate SNRs into two groups. In older remnants, such as the Cygnus Loop (Green 1990), S 147, IC 443 and CTA 1 (Pineault et al. 1997) the high-emissivity parts of the shell tend to have flatter spectral indices than the more diffuse regions. Regions which appear to be "confined" are consistently flatter than the more freely expanding portions of the remnant.

In younger remnants (ages less than "several thousand years"), Anderson & Rudnick (1993) find the situation to be less clear and there is no distinct correlation of spectral index with brightness of the emission. Moffett & Reynolds (1994a,1994b) studied two young SNRs looking for spectral-index variations

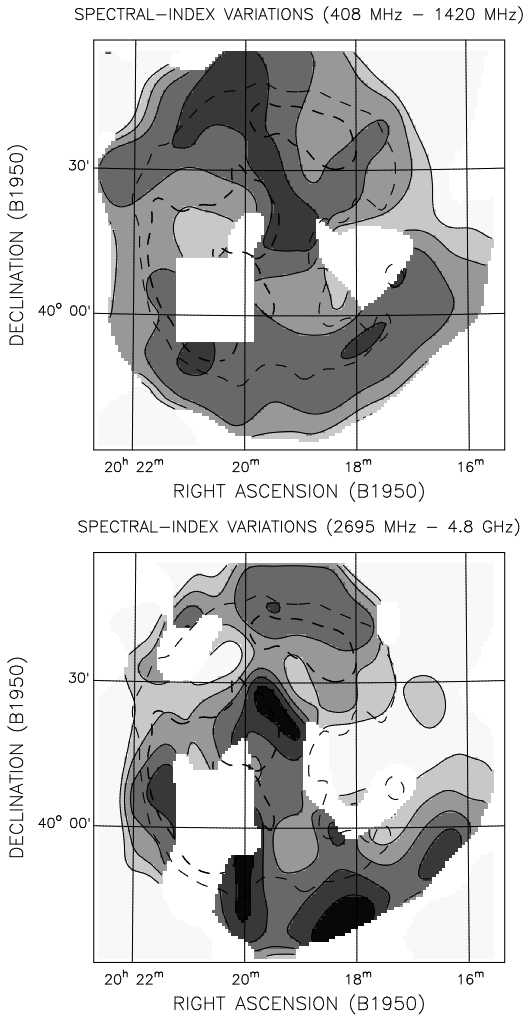

Fig. 8. Maps of differential spectral index where the frequency ratio is in the range of (1.8 – 3.5):1. Details are the same as for Fig. 4.

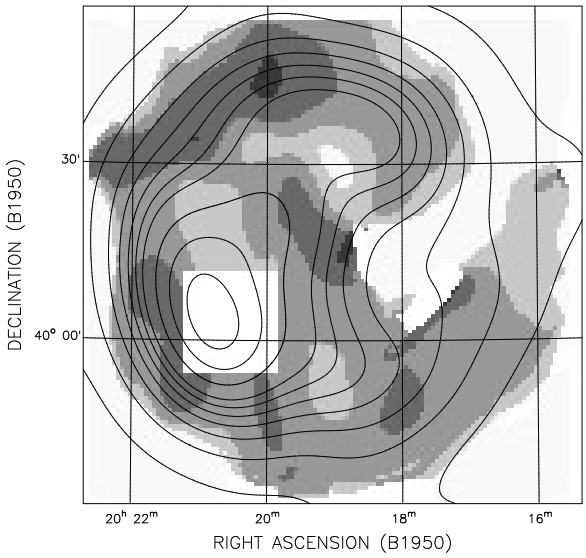

Fig. 9. The average, over all frequency pairs, of the differential spectral index, compared to the 232-MHz brightness-temperature distribution (at the same effective resolution of 14.5′). The five shading levels denote the following ranges of spectral index: (darkest) $>$ 0.7; 0.7 to 0.6; 0.6 to 0.5; 0.5 to 0.4; (lightest) $<$ 0.4. The contours give the smoothed 232-MHz brightness temperature where the contour levels are 100, 250, 500, 750, 1000, 1250, 1500, 2000, 2500 and 3000 K. Every second contour is heavier, with the 2000-K contour heaviest.

correlated with brightness but also found no clear evidence for such an effect.

In G78.2+2.1 there too appears to be no clear variation of spectral index with brightness, with steeper spectral indices being found both in moderately bright regions (the outer edges) and in the fainter central region. Thus it would appear to fall into the "younger remnant" category of Anderson & Rudnick. But is G78.2+2.1 a younger SNR? Higgs et al. (1977) estimated an age between 6000 and 25000 years, for a distance of 1.8 kpc (diameter of 33 pc). However, this estimate was based on the $\Sigma - D$ relationship between surface brightness, Σ, and distance, D, which is no longer thought to be a valid correlation. Landecker et al. (1980) considered several distance indicators and concluded that the distance probably was in the 1 – 2 kpc range. If the SNR were as close as 1 kpc, the diameter could be as small as 18 pc and the age considerably less than 10000 years. Thus G78.2+2.1 could be considered an "adolescent" remnant, if not a young SNR.

The surface brightness of G78.2+2.1 at 1 GHz is Σ_{1GHz} = 1.42×10^{-20} Wm^{-2}Hz^{-1}sr^{-1}. Roughly 20% of the 215 SNRs in the catalog of Green (1996) have a surface brightness greater than 10^{-20} Wm^{-2}Hz^{-1}sr^{-1}. The high surface brightness of G78.2+2.1 is presumably only partially due to its youthfulness. More important may be its interaction with a dense interstellar environment, as verified by the observations of Landecker et al. (1980) and Fukui & Tatematsu (1988).

If the radio emission from G78.2+2.1 were simply due to shock compression of the ambient Galactic magnetic field and the ambient population of relativistic electrons, then the radio spectrum of the SNR should resemble the Galactic synchrotron spectrum, shifted to a higher frequency (by an amount dependent on the compression ratio). Since the Galactic spectrum has a break ($\alpha \sim 0.4$ below 100 MHz and $\alpha \sim 0.8$ above 500 MHz), a similar break would exist in the SNR spectrum. This could result in spectral indices which vary according to the compression. However the fact that the integrated radio spectrum of G78.2+2.1 is linear over the observed range of frequencies does not support such an interpretation. Moreover, based on uniform emission within a spherical volume, the volume emissivity of G78.2+2.1 at 1 GHz is about 1500 times that of the Galactic synchrotron background (for a distance of 1 kpc). Since the emission is probably confined to a shell, the actual ratio would be higher than this. If the shell thickness were 0.2 times the shell radius, the ratio could be as high as 3000. This greatly exceeds any increase in emissivity that could be produced by adiabatic shocks compressing the ambient magnetic field and relativistic

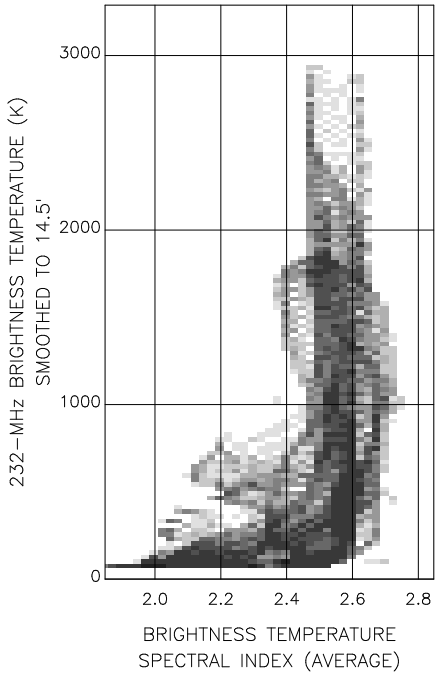

Fig. 10. The distribution of average brightness-temperature spectral index versus 232-MHz brightness temperature, after smoothing to a resolution of $\sim 14.5'$. The comparison of spectral index versus intensity has been made only at positions in the 232-MHz image where the average differential spectral index was well determined. The gray scale indicates the density of the points in the plot.

electrons, but does not entirely rule out radiative shocks where high compression ratios can be achieved.

Therefore, there is strong evidence that the increased emissivity is the result of particle acceleration in the SNR shock. The spectral index variations must reflect differences in the acceleration process from place to place within the SNR.

There is ample evidence that particle acceleration is occuring at the shock front in young SNRs (e.g. Koyama et al. 1995). The particles that are accelerated when the SNR is young are expected to have a long lifetime – 10^5 years or more (Ellison & Reynolds 1991). However, particle acceleration will continue throughout the lifetime of the SNR and the existence of spectral-index variations probably demonstrates that current acceleration of electrons is contributing significantly to the radio emission. (Because of the long lifetime of the accelerated electrons, synchrotron radiation losses can not be an important factor in steepening the electron spectrum).

The generally accepted mechanism of acceleration of particles at the shock front is the first-order Fermi process (e.g. Bell 1978). In the test-particle approximation, this produces an electron spectrum with a power-law exponent of -2.0 for a strong shock, which in turn produces a radio spectral index, α, of 0.5. For weaker shocks (lower compression, lower Mach number), the radio spectral index increases. For a shock with a Mach number as low as 3, the spectral index rises to 0.7. For this reason, the steeper spectral indices in the diffuse fainter regions of old SNRs have been interpreted as evidence of shocks of lower Mach numbers. Pineault et al. (1997) apply this interpretation to CTA 1.

A more self-consistent analysis of shock acceleration (in which the back-reaction on the shock of the accelerated particles themselves is included) by Ellison and Reynolds (1991) has shown that a curved electron spectrum results (which differs from the accelerated proton spectrum). As a consequence, the resulting radio spectrum is also curved and the deduced spectral index may depend upon the strength of the compressed magnetic field in the emitting region. Variations of 0.1 in α are possible. Based on this model, spectral indices of ~ 0.64 in the Tycho and Kepler SNRs can be accounted for, even for strong shocks. The steeper spectral indices around the periphery of G78.2+2.1 may reflect regions of stronger magnetic field, but the lack of a correlation between spectral index and brightness casts doubt on this interpretation. It is also difficult to interpret them as evidence of weaker shocks.

On the other hand, Dröge et al. (1987) proposed that second-order Fermi processes could moderate the spectral-index increases predicted in the test-particle case for lower-Mach-number shocks, and could even account for values of $\alpha < 0.5$ if the pre-shock gas is magnetic-field dominated (Schlickeiser & Fürst 1989). However, this applies only for a parallel shock and this effect would be most common in young SNRs where the magnetic field is predominantly radial; we have shown above that G78.2+2.1 has probably advanced beyond this stage in its evolution.

It is unclear whether any of these theoretical predictions can be applied to the spectral-index variations in G78.2+2.1. The main value of the present observations lies in the clear evidence of spectral-index variations, and the strong indication that steeper spectral indices seem to occur towards the outside of the regions of strongest radio emission.

It should be noted that Brazier et al. (1996) have found an X-ray point source near the centre of G78.2+2.1 (coincident within the errors with the γ-ray source 2EG J2020+4026. The X-ray source lies within the region of steeper spectral index seen towards the (projected) centre of the remnant. It is possible that this is evidence of a central compact object, but the usual result of activity from such an object is a flat-spectrum region. It is more likely that the steeper-spectrum radio emission is actually being generated at the periphery of the SNR and is only seen at the centre due to projection.

6. Conclusions

A new value of the integrated flux density of G78.2+2.1 at 232 MHz has been derived, 670 ± 50 Jy, using a new total intensity map which has good dynamic range. A multi-frequency study of integrated spectral index of G78.2+2.1 using the method of T–T plots gives a value of 0.54 ± 0.02, over a wide range of frequencies, assuming accurate brightness-temperature scales for the various observations that were used. There is some weak thermal emission mixed with the non-thermal emission from the

SNR, aside from the strong thermal source, the γ-Cygni Nebula, which was removed from the region of analysis.

Spatial spectral variations over the supernova remnant are found to be of the order of$\pm$ 0.15 in α. Although variations of this order have been reported in other SNRs, this is the first study that has used as many as five frequencies. A consistent pattern of such variations appears for all pairs of frequency combinations. Some of these variations (towards lower values of α) are possibly due to the blending of thermal and non-thermal emission. A patch of higher spectral index has been found near the centre of the remnant (although it may be physically located in the remnant's shell), and steeper-spectrum regions appear around the shock periphery of the SNR. No strong correlation of spectral indices with intensity was found. No clear theoretical interpretation of these features has been found.

Studies similar to this one of other SNRs would be valuable in searching for systematic patterns of spectral-index variation.

Acknowledgements. Zhang and Zheng wish to acknowledge the contributions of all their colleagues in the Miyun meter-wave radio astronomy group. It is their collective effort that has made the operation of the MSRT successful. This work was supported partly by the Chinese Academy of Sciences. Zhang and Zheng also thank the DRAO staff for the kind hospitality during their stay at Penticton. The DRAO Synthesis Telescope is operated by the National Research Council of Canada as a national facilty for radio astronomy.

References

Anderson, M.C., Rudnick, L., 1993, ApJ 408, 514
Baars, J.W.M., Genzel, R., Pauliny-Toth, I.I.K., Witzel, A., 1977, A&A 61, 99
Baars, J.W.M., Genzel R., Pauliny-Toth, I.I.K., Witzel, A., 1977, A&A 61, 99
Bell, A.R., 1978, MNRAS 182, 147
Braun, R., Walterbos, R.A.M., 1985, A&A 143, 307
Braun, R., Strom, R.G., 1986, A&AS 63, 345
Brazier, K.T.S., Kanbach, G., Carramiñana, A., Guichard, J., Merck, M., 1996, MNRAS, 281, 1033
Costain, C.H., 1960, MNRAS 120, 248
Dröge, W., Lerche, I., Schlickeiser, R., A&A, 178, 252
Ellison, D.C., Reynolds, S.P., 1991, ApJ 382, 242
Fukui, Y., Tatematsu, K., 1988, in "Supernova Remnants and the Interstellar Medium", IAU Coll. 101, eds. R.S. Roger, T.L. Landecker, Cambridge Univ. Press, p. 261
Fürst, E., Reich, W., Reich, P., Reif, K., 1990, A&AS 85, 691
Gray, A., Landecker, T.L., 1997, in preparation
Green, D.A., 1990, AJ 100, 1927
Green, D.A., 1996, "A Catalogue of Galactic Supernova Remnants (1996 August version)", Mullard Radio Astronomy Observatory, Cambridge, U.K. (available on World Wide Web at "http:/www.mrao.cam.ac.uk/surveys/snrs/"")
Higgs, L.A., 1977, AJ 82, 329
Higgs, L.A., Landecker, T.L., Roger, R.S., 1977, AJ 82, 718
Higgs, L.A., Landecker, T.L., Roger, R.S., 1983, AJ 88, 97
Higgs, L.A., Landecker, T.L., Seward, F.D., 1983, in "Supernova Remnants and Their X-ray Emission", IAU Symp. 101, eds. J. Danziger, P. Gorenstein, Reidel, Dordrecht, p. 281
Koyama, K., Petre, R., Gotthelf, E.V., Hwang, U., Matsuura, M., Ozaki, M., Holt, S.S., 1995, Nature, 378, 255
Landecker, T.L., Roger, R.S., Higgs, L.A., 1980, A&AS 63, 345
Landecker, T.L., Zhang, X., Zheng, Y., Higgs, L.A., 1996, A&A, submitted
Leahy, D.A., Roger, R.S., 1991, AJ 101, 1033
Moffett, D.A., Reynolds, S.P., 1994a, ApJ 425, 668
Moffett, D.A., Reynolds, S.P., 1994b, ApJ 437, 705
Pineault, S., Chastenay, P., 1990, MNRAS 246, 169
Pineault, S., Landecker, T.L., Swerdlyk, C.M., Reich, W., 1997, A&A, in press
Roger, R.S., Costain, C.H., Lacey, J.D., Landecker, T.L., Bowers, F.K., 1973, Proc. IEEE 61, 1270
Schlickeiser, R., Fürst, E., 1989, A&A, 219, 192
Turtle, A.J., Pugh, J.F., Kenderdine, S., Pauliny-Toth, I.I.K., 1962, MNRAS 124, 297
Veidt, B.G., Landecker, T.L., Vaneldik, J.F., Dewdney, P.E., Routledge, D., 1985, Radio Science 20, 1118
Wendker, H.J., 1984, A&AS 58, 291
Wendker, H.J., Higgs, L.A., Landecker, T.L., 1991, A&A 241,551
Zhang, X., 1995, Publ. Shanghai Obs., in press
Zhang, X., Zheng, Y., Chen, H., Wang, S., 1993, A&AS 99, 545
Zheng, Y., 1989, Chinese Science Bulletin 34, 1020

This article was processed by the author using Springer-Verlag LaTeX A&A style file *L-AA* version 3.